INL/CON-15-36793
PREPRINT

Newton-Krylov Method in Applications of Solving Two-phase Problems using Drift Flux Model

International Congress on Advances in Nuclear Power Plants (ICAPP 2016)

Ling Zou, Haihua Zhao, Hongbin Zhang

November 2015

The INL is a
U.S. Department of Energy
National Laboratory
operated by
Battelle Energy Alliance

NEWTON-KRYLOV METHOD IN APPLICATION OF SOLVING TWO-PHASE PROBLEMS USING DRIFT FLUX MODEL

Ling Zou, Haihua Zhao, Hongbin Zhang
Idaho National Laboratory, USA
Idaho National Laboratory: PO BOX 1625, Idaho Falls, ID 83415-3870, USA

In this paper, Jacobian-free Newton-Krylov (JFNK) method is investigated in an application to implicitly solve two-phase flow problems using four-equation drift flux model. The closure models include the EPRI drift flux correlations and additional constitutive models to determine flow regimes, wall boiling and interfacial heat/mass transfer, two-phase flow wall friction, etc. Different from many traditional computer codes, fully implicit methods are used for the time integration. The resulted nonlinear discretized equation system is solved using the JFNK method. Expensive and error-prone derivation and implementation of the analytical Jacobian matrix are avoided. Numerical results are successfully validated using existing experimental data on flow boiling under forced convection conditions in both pipe and rod bundle geometries.

I. INTRODUCTION

Accurate modeling and simulation of the two-phase flow phenomena are critical to the safety analysis of nuclear reactors. In reactor safety analysis, two-phase flow problems can generally be formulated using drift flux models or two-fluid models. Compared to the more complex two-fluid six-equation model, the drift flux models (Refs. 1-3) treat the two phases as a mixture, and the relative motion between the two phases is treated by constitutive correlations. Although the drift flux models have limitations in certain applications, they are widely used in many applications due to their simplicity and applicability to a wide range of two-phase flow problems. For example, the RETRAN-3D (Ref. 4) code uses the drift flux models and has many applications in reactor transient analyses including a small break loss of coolant accident. The TASS/SMR system analysis code is developed based on a three-equation drift flux model (with an additional mass equation for the non-condensable gas) for the system integrated modular advanced reactor, SMART (Refs. 5, 6). Drift flux models have also been widely used in the subchannel analysis of boiling water reactor (BWR) fuel bundles (Refs. 7-9), BWR core simulators (Ref. 10), and two-phase flow instabilities analyses (Refs. 11, 12).

In recent years, the Jacobian-free Newton-Krylov (JFNK) method has gained increasing interest in solving nonlinear problems. Mousseau has done several pioneering work (Refs. 13, 14) to investigate the JFNK method in solving two-phase flow problems. It has also been applied as the main solver for the system analysis code, RELAP-7, being developed at Idaho National Laboratory (Refs. 15, 16), and for the multi-physics simulations of nuclear reactors (Ref. 17). In our previous work, the JFNK method has been extensively investigated to solve two-phase flow problems using both the drift flux model (Ref. 18) and the two-fluid model (Refs. 19-21). In most of these work, only simplified and continuous closure models have been used, with the exception of the previous work on drift flux model (Ref. 18). In our previous work (Ref. 18), constitutive correlations for the drift flux model are provided in three vertical two-phase flow regimes (bubbly, slug and annular mist flow regimes) as discontinuous functions. Similar to existing system analysis codes, a transitional regime between the slug and the annular mist flow regimes had to be used to avoid numerical difficulty, such as code non-convergence. A linear interpolation of drift flux constitutive correlations was used in this transitional regime. However, although linear interpolation of correlations was used, unexpected and unsatisfactory nonlinear behaviors were observed in the results (void fraction vs. equilibrium quality plot).

This work represents an extension to our previous work (Ref. 18) by implementing the EPRI drift flux correlations (Ref. 22) under the JFNK framework. The EPRI model was developed as an empirical model that eliminates the need to know the flow regime before void fraction prediction. More importantly, the correlations are continuous functions that could greatly improve the effectiveness of a Newton type of solving scheme, such as the JFNK method used in this work. Section II provides model descriptions for the drift flux flow equation model along with the EPRI drift flux correlations, as well as additional constitutive correlations required to fully close the system, such as wall boiling and two-phase flow pressure drop. Section III presents the numerical schemes for space and time to discretize the drift flux flow equation model. A brief introduction to the JFNK method is also included. Section IV presents the validation of the code using flow boiling experimental data in vertical tubes and rod bundles. Additional discussions and conclusions are presented in Section V.

II. MODEL DESCRIPTIONS

II.A. Four-Equation Drift Flux Model

The one-dimensional four-equation drift flux model used in this work is the same as used in our previous work (Ref. 18). The original set of equations for the one-dimensional drift flux model includes two continuity equations (mixture and the dispersed phase), one mixture momentum equation and one mixture energy equation (Refs. 3, 23). This original set of equations has been simplified and is given as Eqs. (1)–(4):

$$\frac{\partial \rho_m}{\partial t} + \frac{\partial (\rho_m v_m)}{\partial x} = 0 \tag{1}$$

$$\frac{\partial (\alpha \rho_g)}{\partial t} + \frac{\partial (\alpha \rho_g v_m)}{\partial x} + \frac{\partial}{\partial x}\left(\frac{\alpha \rho_g \rho_f}{\rho_m}\overline{V_{gJ}}\right) = \Gamma_g \tag{2}$$

$$\begin{aligned}\frac{\partial v_m}{\partial t} + v_m \frac{\partial v_m}{\partial x} = &-\frac{1}{\rho_m}\frac{\partial p}{\partial x} - g_x - \frac{f_m}{2D} v_m |v_m| \\ &- \frac{1}{\rho_m}\frac{\partial}{\partial x}\left[\frac{\alpha \rho_g \rho_f}{(1-\alpha)\rho_m}\overline{V_{gJ}}^2\right]\end{aligned} \tag{3}$$

$$\begin{aligned}\frac{\partial (\rho_m e_m)}{\partial t} + \frac{\partial (\rho_m h_m v_m)}{\partial x} + \frac{\partial}{\partial x}\left[\frac{\alpha \rho_g \rho_f}{\rho_m}\Delta h_{gf}\overline{V_{gJ}}\right] \\ = q''_w a_w \\ + \left[v_m + \frac{\alpha(\rho_f - \rho_g)}{\rho_m}\overline{V_{gJ}}\right]\frac{\partial p}{\partial x}\end{aligned} \tag{4}$$

in which the subscripts m, g and f denote the two-phase mixture, gas phase, and liquid phase, respectively. $\overline{V_{gJ}}$ is the mean drift velocity of the gas phase. q''_w is the prescribed heat flux on the wall, and a_w is the volumetric heating surface density. Comparing to the original equations (Refs. 3, 23), there are several noticeable changes that need explanations: (1) the mixture momentum equation has been rewritten in the primitive form, which was done in a similar way to obtain the primitive momentum equation for the single-phase Euler equations; (2) in the mixture energy equation, the two transient terms of enthalpy and pressure were combined to obtain the transient term of the internal energy; (3) the stress tensor was simplified and integrated into 1-D friction term, and covariance terms were ignored; and (4) the drift terms in the gas phase mass equation and the mixture energy equation have been moved to the left-hand side of the equations, which will be treated as advection terms in the numerical implementations.

The primary variables to be solved from this set of equations are p, α, v_m, and T, which are pressure, void fraction (volume fraction of the gas phase), mixture velocity, and temperature, respectively. It is noted that the phasic temperatures, T_l and T_g, have not been properly defined yet. There are two possible choices for defining the phasic temperatures. For one choice, it is assumed that the phasic temperatures are the same, such that, $T_f = T_g = T$. For the other choice, the vapor phase is always at the saturation condition, such that $T_g = T_{sat}(p)$ and the liquid phase temperature can deviate from the saturation temperature (e.g., subcooled liquid) and $T_f = T$. For flow boiling problems, it is obvious that the later choice is more appropriate. For example, under subcooled flow boiling conditions, it is incorrect to assume that the vapor temperature is the same as the (subcooled) liquid temperature.

Additional closure correlations are included in the following sections to describe the criteria for flow regime transitions, two-phase pressure drop coefficients, wall boiling model, and interfacial heat transfer coefficients, etc.

II.B. EPRI Drift Flux Correlation

The four-equation drift flux model described in Eqs. (1)–(4) are closed with additional closure correlations for the distribution parameter C_0, and the weighted mean drift velocity of the gas phase, V_{gj}. In this work, the EPRI drift flux closure correlations were used to determine these two parameters. The ERPI drift flux closure correlations were originally developed by Chexal and Lellouche (Ref. 22), and a modified version was later developed and adopted in the RELAP5-3D code (Ref. 24). The later version used in the RELAP5-3D code is adopted in this work. The EPRI drift flux closure correlations cover a wide range of pressure, flow, and void fraction conditions. The distribution parameter, C_0, is calculated from,

$$C_0 = \frac{L}{K_0 + (1 - K_0)\alpha^r} \tag{5}$$

The weighted mean drift velocity of the gas phase, V_{gj}, is calculated from,

$$V_{gj} = 1.41\left[\frac{(\rho_f - \rho_g)\sigma g}{\rho_f^2}\right]^{1/4} C_1 C_2 C_3 C_4 \tag{6}$$

For simplicity, the detailed explanations of Eqs. (5) and (6) are omitted, and interested readers are referred to the RELAP5-3D code manual (Ref. 25). An additional correlation is provided to close the drift flux equation system (Ref. 18),

$$\overline{V_{gJ}} = \frac{\rho_m V_{gj} + \rho_m (C_0 - 1) v_m}{\rho_m - (C_0 - 1)\alpha(\rho_f - \rho_g)} \tag{7}$$

It is noted that, phasic velocities are required to compute V_{gj}. However, phasic velocities can be only calculated after $\overline{V_{gJ}}$ being updated. Therefore, an internal iteration algorithm is implemented to update V_{gj} and phasic

velocities simultaneously in the code. A major difference between the EPRI correlations and those proposed by Hibiki and Isshi (Ref. 23) is that the EPRI correlations provide continuous functions covering the whole two-phase flow regions without the need to determine two-phase flow regime beforehand. Therefore, a transitional flow regime between the slug and annular mist flow regimes, necessary in our previous work (Ref. 18) to avoid numerical difficulty, is eliminated. As a result, the Newton-Krylov solver showed better convergence in solving the two-phase flow problems, and numerical results obtained agree with experimental data much better. This will be discussed in section V with more details.

II.C. Net Vapor Generation Rate

Similar to RELAP5-3D (Ref. 24), the net vapor generation rate under wall boiling conditions is modeled in two regions, the near wall and bulk region,

$$\Gamma_g = \Gamma_w + \Gamma_{ig} \tag{8}$$

The net vapor generation rate in the near wall region, Γ_w, is determined using the method proposed by Lahey, and the Saha-Zuber correlation in determining the onset point of net vapor generation (Ref. 24). The vapor generation rate in the bulk region is determined by the heat transfer between the two phases and interface, which is assumed to be at the saturation condition. For single-phase liquid and boiling conditions considered in this work, the gas phase is assumed to be always at the saturation condition, and thus the volumetric vapor generation in the bulk region is reduced to:

$$\Gamma_{ig} = \frac{H_{il}(T_l - T_{sat})}{h_{fg}} \tag{9}$$

in which, H_{il} is the volumetric interfacial heat transfer coefficient for the liquid phase. This parameter is also flow regime dependent, and the RELAP5-3D constitutive correlations are used (see Section 4.1 of Ref. 25).

II.D. Frictional Pressure Drop

Frictional pressure drop correlations used in this work are mainly based on those used in RELAP5-3D (Ref. 24). The single-phase flow frictional factor is calculated in three flow regimes, laminar flow, turbulent flow and a transition region between these two. The two-phase flow frictional pressure drop is based on a two-phase multiplier approach, which is,

$$\left(\frac{dp}{dx}\right)_{two\_phase} = \phi_f^2 \left(\frac{dp}{dx}\right)_f = \phi_g^2 \left(\frac{dp}{dx}\right)_g \tag{10}$$

In the context of the drift flux model, the wall friction term in the momentum equation becomes,

$$\frac{f_m}{2D} v_m |v_m| = \frac{1}{\rho_m}\left(\frac{dp}{dx}\right)_{two\_phase} \tag{11}$$

in which, ϕ_f and ϕ_g are the liquid-alone and vapor/gas-alone two-phase Darcy-Weisbach friction multipliers, respectively. More details of the implementations of frictional pressure drop can be found in Section 3.3.8 of Ref. 24.

III. NUMERICAL METHODS

In this section, numerical discretization schemes and solution methods are discussed, including: 1) the finite volume discretization scheme based on the staggered grid mesh arrangement; 2) the first-order fully implicit backward Euler time integration scheme; and 3) the JFNK method to solve the nonlinear equation system.

III.A. Finite volume method

In this work, the finite volume method based on the staggered grid mesh has been used for the spatial discretization of the equation system. For the staggered grid mesh arrangement, scalar variables (such as pressure, void fraction, and temperature) are arranged at the cell centers, while vector variables (such as mixture velocity) are arranged at the cell edges, which are schematically shown in Fig. 1.

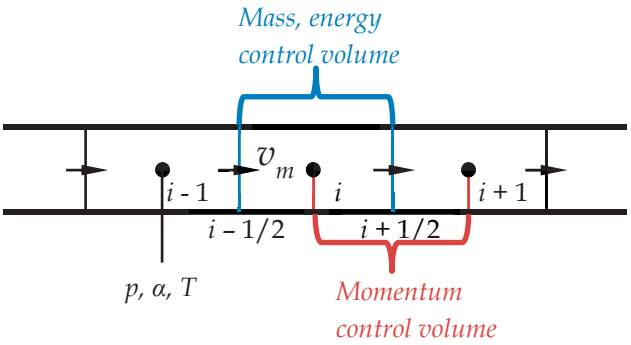

Fig. 1. Schematic drawing of the staggered grid mesh arrangement.

With pressure, void fraction, and temperatures being defined at the cell centers, phasic thermodynamic quantities are also defined at the cell centers and calculated from the water/steam properties functions. For example, the liquid density at the i^{th} volume is calculated as:

$$\rho_{f,i} = \rho_f(p_i, T_{f,i}) \tag{12}$$

Similarly, the mixture thermodynamic properties are also defined at the cell centers and calculated from their definitions, for example:

$$\rho_{m,i} = \alpha_i \rho_{g,i} + (1 - \alpha_i)\rho_{f,i} \tag{13}$$

It is worth noting that the weighted mean drift velocity of the gas phase (V_{gj}) and the distribution parameter (C_0) are generally correlated with local phasic thermodynamic properties and void fraction, etc., and therefore both have been defined at the cell centers:

$$V_{gj,i} = V_{gj}(\alpha_i, \rho_{f,i}, \rho_{g,i}, \dots) \tag{14}$$

$$C_{0,i} = C_0(\alpha_i, \rho_{f,i}, \rho_{g,i}, \dots) \tag{15}$$

Consequently, the mean drift velocity of the gas phase, $\overline{V_{gJ}}$, is also defined at the cell centers. When the value of a variable is required at the cell centers (or cell edges), but the variable is not defined there, an arithmetic average is used, for example,

$$\rho_{m,i+1/2} = \frac{1}{2}(\rho_{m,i+1} + \rho_{m,i-1}) \tag{16}$$

$$v_{m,i} = \frac{1}{2}(v_{m,i-1/2} + v_{m,i+1/2}) \tag{17}$$

In this work, all advection terms (including those due to drift) in the equations are treated similarly using the classic donor cell concept. It is a first-order but very stable spatial discretization scheme. Using the gas phase mass equation as an example, the mixture advection term on the left-hand side of the equation is discretized as:

$$\left.\frac{\partial(\alpha\rho_g v_m)}{\partial x}\right|_i = \frac{1}{\Delta x}\left[(v_m\alpha\rho_g)^*_{i+1/2} - (v_m\alpha\rho_g)^*_{i-1/2}\right] \tag{18}$$

and

$$(v_m\alpha\rho_g)^*_{i+1/2} = v_{m,i+1/2}\begin{cases}\alpha_i\rho_{g,i} & if \quad v_{m,i+1/2} > 0\\ \alpha_{i+1}\rho_{g,i+1} & otherwise\end{cases} \tag{19}$$

The drift term is also numerically treated as an advection term, and thus:

$$\frac{\partial}{\partial x}\left(\frac{\alpha\rho_g\rho_f}{\rho_m}\overline{V_{gJ}}\right)_i = \frac{1}{\Delta x}\left[\left(\frac{\alpha\rho_g\rho_f}{\rho_m}\overline{V_{gJ}}\right)^*_{i+1/2} - \left(\frac{\alpha\rho_g\rho_f}{\rho_m}\overline{V_{gJ}}\right)^*_{i-1/2}\right] \tag{20}$$

and

$$\left(\frac{\alpha\rho_g\rho_f}{\rho_m}\overline{V_{gJ}}\right)^*_{i+1/2} = \left.\overline{V_{gJ}}\right|_{i+1/2}\begin{cases}\dfrac{\alpha_i\rho_{g,i}\rho_{f,i}}{\rho_{m,i}} & if \quad \left.\overline{V_{gJ}}\right|_{i+1/2} > 0\\ \dfrac{\alpha_{i+1}\rho_{g,i+1}\rho_{f,i+1}}{\rho_{m,i+1}} & otherwise\end{cases} \tag{21}$$

The advection term and drift term in the energy equation can be treated similarly. The advection term of the mixture momentum equation is treated slightly differently as it is expressed in the primitive form, for example,

$$v_m\left.\frac{\partial v_m}{\partial x}\right|_{i+1/2} = \frac{1}{\Delta x}v_{m,i+1/2}\begin{cases}v_{m,i+1/2} - v_{m,i-1/2} & if\, v_{m,i+1/2} > 0\\ v_{m,i+3/2} - v_{m,i+1/2} & otherwise\end{cases} \tag{22}$$

For all other source terms appearing in the equation, the central differencing scheme is used when a gradient appears.

For boundary conditions, given liquid phase inlet mass flux $G_{f,inlet}$, vapor phase inlet mass flux, $G_{g,inlet}$, and inlet temperatures are considered in this work. For the flow boiling simulations with subcooled inlet conditions, $G_{g,inlet}$ is set to be zero. However, the following derivations are based on nonzero assumptions, representing a general case. Under these conditions, the inlet boundary condition for the mixture mass equation is computed as:

$$(\rho_m v_m)_{inlet} = G_{f,inlet} + G_{g,inlet} \tag{23}$$

For the vapor mass equation, the inlet boundary condition is given by:

$$\left(\alpha\rho_g v_m + \frac{\alpha\rho_g\rho_f}{\rho_m}\overline{V_{gJ}}\right)_{inlet} = G_{g,inlet} \tag{24}$$

For the mixture energy equation, the inlet boundary condition is given by:

$$\left(\rho_m h_m v_m + \frac{\alpha\rho_g\rho_f}{\rho_m}\Delta h_{gf}\overline{V_{gJ}}\right)_{inlet} = G_{f,inlet}h_{f,inlet} + G_{g,inlet}h_{g,inlet} \tag{25}$$

where, $h_{f,inlet}$ and $h_{g,inlet}$ are the specific enthalpy for the liquid and gas phase evaluated at the inlet, respectively. When evaluating these two parameters, the inlet temperatures are normally given and the inlet pressure comes from the numerical iterations (i.e., the inlet pressure is part of the unknowns of the system). For the outlet, an outlet pressure boundary is normally used for the momentum equation.

III.B. Time integration schemes

The fully implicit backward Euler (BDF1) time integration scheme is used this work. Using the mixture phase continuity equation as an example, the semi-discretized form is expressed as,

$$\frac{\rho_m^{n+1} - \rho_m^n}{\Delta t} + \frac{\partial(\rho_m v_m)^{n+1}}{\partial x} = 0 \tag{26}$$

in which, Δt is the time step size, and superscripts n and n+1 denote the old time step and current time step, respectively.

III.C. Jacobian-free Newton-Krylov Method

Using the finite volume spatial discretization and the BDF1 time integration scheme, the drift flux model equations can be discretized into a set of nonlinear equations, which is solved using JFNK. This method has been widely used and tested in our previous studies. This section provides a briefly discussion on the JFNK method. For a discretized nonlinear system, one solves:

$$\boldsymbol{F}(\boldsymbol{U}) = 0 \tag{27}$$

for the unknown vector, $\boldsymbol{U}$, which is $[\ldots, p_i, \alpha_i, T_i, v_{m,i+1/2}, \ldots]^T$ for the drift flux model studied in this work. The solution to the nonlinear system is obtained by iteratively solving a series of Newton's linear correction equations:

$$\boldsymbol{J}^k \delta \boldsymbol{U}^k = -\boldsymbol{F}(\boldsymbol{U}^k) \tag{28}$$

where, $\boldsymbol{J}^k$ is the Jacobian matrix; $\boldsymbol{U}^k$ is the k^{th} nonlinear step solution; and $\delta \boldsymbol{U}^k$ is the correction vector. In the JFNK frame, the linear system, Equation (28), could be effectively solved with a Krylov's method. In the Krylov's method, only a matrix-vector product is required and can be approximated as,

$$\boldsymbol{J}^k \boldsymbol{v} \approx \frac{\boldsymbol{F}(\boldsymbol{U}^k + \epsilon \boldsymbol{v}) - \boldsymbol{F}(\boldsymbol{U}^k)}{\epsilon} \tag{29}$$

in which, $\boldsymbol{v}$ is the Krylov vector. After the correction vector, $\delta \boldsymbol{U}^k$, is solved from the linear system, the $(k+1)^{\text{th}}$ nonlinear step solution could be updated as:

$$\boldsymbol{U}^{k+1} = \boldsymbol{U}^k + \delta \boldsymbol{U}^k \tag{30}$$

One of the advantages of using the JFNK method is that the explicit formation of the Jacobian matrix could be avoided. The derivation and code implementations of the analytical Jacobian matrix could be a cumbersome and error-prone task for two-phase flow problems, since many thermal-hydraulics correlations have quite complicated forms. In our implementation of the JFNK method, the scientific computational toolkit PETSc (Ref. 26) is used to solve the discretized nonlinear fluid equations.

IV. RESULTS AND DISCUSSIONS

This section presents code validation by comparing the numerical results with the experimental data. Additional comparisons between results obtained in this work and those obtained in our previous work (Ref. 18) are also presented to demonstrate the significant improvement made in this work.

Bartolomei experimental data of subcooled flow boiling in vertical round pipes (length 1.5 m, pipe I.D. 0.012m) (Ref. 27) and FRIGG experimental data of flow boiling in vertical rod bundles (length 4.365m, 36 rods) (Ref. 28) have been chosen for the purpose of validation in this work. These two experiments (only for those data used in this work) cover wide ranges of thermal-hydraulics conditions: pressure from 3 to 15 MPa, mass flux from 405 to 2123 kg/(m^{2}s), wall heat flux from 0.42 to 2.21 MW/m^2, and maximum outlet void fraction up to 0.9. A summary of all experimental conditions is provided in TABLE I for the Bartolomei data, and TABLE II for the FRIGG data, respectively. In both experiments, void fraction data were measured at steady state conditions. It was reported that the maximum absolute errors of the void fraction measurements do not exceed 0.04 for the Bartolomei data (Ref. 27), and 0.003 for the FRIGG data (Ref. 28). For all the simulation cases, 40 finite volume cells are used. Steady-state solutions were obtained at the end of transient simulations using a time step of 0.02 s, and 100 time steps. The computational cost for each simulation is in the order of 1 second of computer time, using 2.8 GHz Intel Core i7 CPU.

The mean absolute error (MAE) is used to quantify the error between numerical results and experimental measurements. In this case, the mean absolute error is defined as,

$$\varepsilon_\alpha = \frac{1}{N}\sum_{i=1}^{N} \left| \alpha_{num,i} - \alpha_{exp,i} \right| \tag{31}$$

in which, subscripts '*num*' and '*exp*' denote for numerical results and experimental data, respectively. Interpolation of numerical results is used when necessary. N is the total data number in the two-phase region. It is noted that data only in two-phase flow region are included for error analysis. Mean absolute errors for both Bartolomei and FRIGG cases are summarized in TABLE III. Overall, the numerical results were found to agree well with the experimental data.

The comparisons between the numerical and experimental results are plotted in Figures 2–7 for both the Bartolomei test cases, and in Figures 8–10 for the FRIGG test cases in different groups. For the Bartolomei data, experimental data on void fraction were provided at different local equilibrium quality; and for the FRIGG data, void fraction data were provided at different axial locations. Fig. 2 shows a group of Bartolomei data with similar thermal-hydraulics conditions. It is noted that data scattering is observed in experimental data but not in numerical simulation results due to its deterministic nature. Fig. 3 shows a different group of Bartolomei data with similar pressure (around 7 MPa) and mass flux but with increasing wall heat flux and inlet subcooling. Fig. 8–10 show the comparison between the numerical and experimental results for the FRIGG test cases in different

groups, from which good agreements were observed. Relatively larger discrepancies between the numerical and experimental results were also observed for several cases, for example Bartolomei cases 15, 18, and 24. For these cases, although absolute errors are larger, the void fraction to equilibrium slopes predicted from simulations are similar to those observed in experiments. This suggests that there might be a larger uncertainty associated with the model in predicting the onset of net vapor generation point.

As discussed in the previous sections, by using the ERPI drift flux correlations, the Newton-Krylov solver showed better code convergence, because continuous functions are used. The numerical results obtained in this work are also better by eliminating a transitional flow regime between the slug and annular mist flow regimes, because linear interpolation is unnecessary. In our previous work (Ref. 18), spurious jumps in cases 8, 22, and 23, as marked in Fig. 11, were observed in this transitional regime. On the contrary, numerical results obtained in this work shows much improved behavior without those spurious jumps.

TABLE I. Experimental Conditions of the Bartolomei Flow Boiling Tests in Vertical Pipes (Ref. 27)

Case	P (MPa)	Mass flux (kg/m^2-s)	Heat flux (MW/m^2)	T_{inlet} (K)
1	6.89	985	1.13	464
2	6.78	1071	1.13	465
3	6.84	961	1.13	465
4	6.84	995	1.15	466
5	6.81	998	0.44	521
6	6.89	965	0.78	493
7	6.84	961	1.13	466
8	6.74	988	1.7	416
9	7.01	996	1.98	434
10	14.79	1878	0.42	603
11	14.74	1847	0.77	598
12	14.75	2123	1.13	583
13	14.7	2014	1.72	545
14	14.99	2012	2.21	563
15	6.89	405	0.79	421
16	6.89	1467	0.77	519
17	6.79	2024	0.78	520
18	11.02	503	0.99	494
19	10.81	966	1.13	502
20	10.81	1554	1.16	563
21	10.84	1959	1.13	563
22	3.01	990	0.98	445
23	4.41	994	0.9	463
24	14.68	1000	1.13	533
25	6.81	2037	1.13	504

TABLE II. Experimental Conditions of the FRIGG Flow Boiling Tests in a Vertical Rod Bundle (Ref. 28)

Case	P (MPa)	Mass flux (kg/m^2-s)	Heat flux (MW/m^2)	$\Delta T_{sub,inlet}$ (K)
413-127	3.00	524	0.217	3
413-145	3.00	1110	0.439	3
413-147	3.00	755	0.664	3.1
413-149	3.03	514	0.439	25.2
413-109	5.00	992	0.664	3.3
413-117	4.98	520	0.439	30.4
413-118	5.00	736	0.664	2.9
413-125	7.00	950	0.664	15.3
413-140	8.68	1606	0.738	2.3
413-141	8.68	981	0.439	2.3

TABLE III. Mean Absolute Error (MAE) of Void Fraction, ε_α, Between Numerical Results and FRIGG FT-36b Experimental Data

Case	MAE	Case	MAE	Case	MAE
1	0.023	13	0.010	25	0.026
2	0.067	14	0.019	413-127	0.067
3	0.038	15	0.115	413-145	0.052
4	0.031	16	0.032	413-147	0.025
5	0.006	17	0.025	413-149	0.023
6	0.049	18	0.065	413-109	0.012
7	0.035	19	0.034	413-117	0.025
8	0.023	20	0.045	413-118	0.028
9	0.015	21	0.019	413-140	0.030
10	0.037	22	0.010	413-141	0.024
11	0.016	23	0.032		
12	0.012	24	0.062		

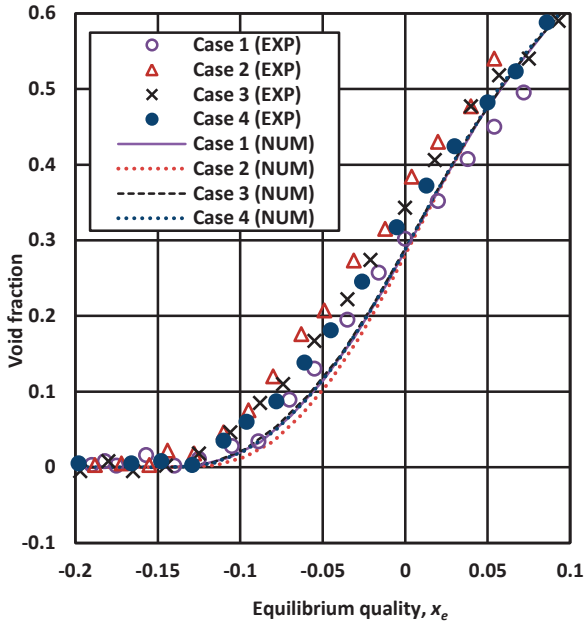

Fig. 2. Comparisons between numerical results (NUM) and experimental measurements (EXP), Group 1.

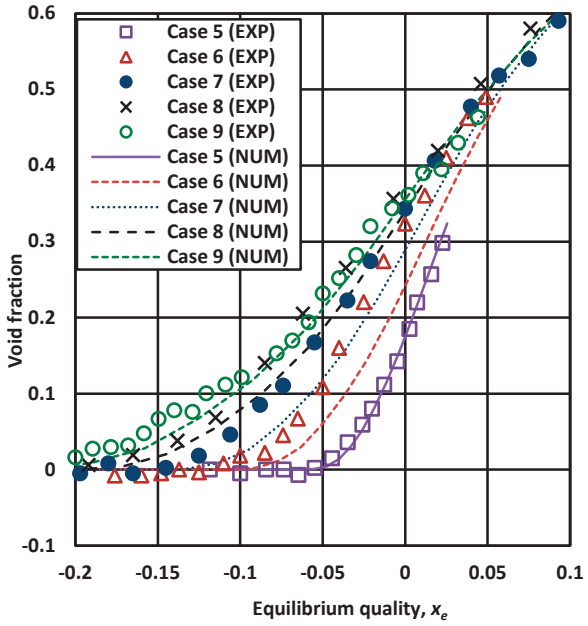

Fig. 3. Comparisons between numerical results (NUM) and experimental measurements (EXP), Group 2.

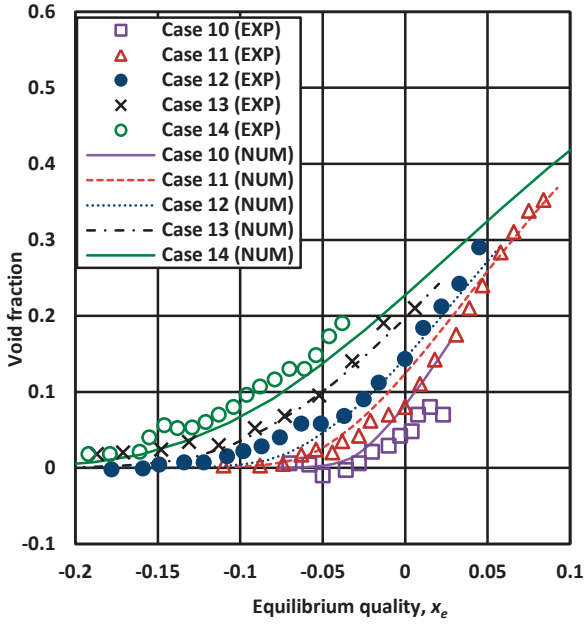

Fig. 4. Comparisons between numerical results (NUM) and experimental measurements (EXP), Group 3.

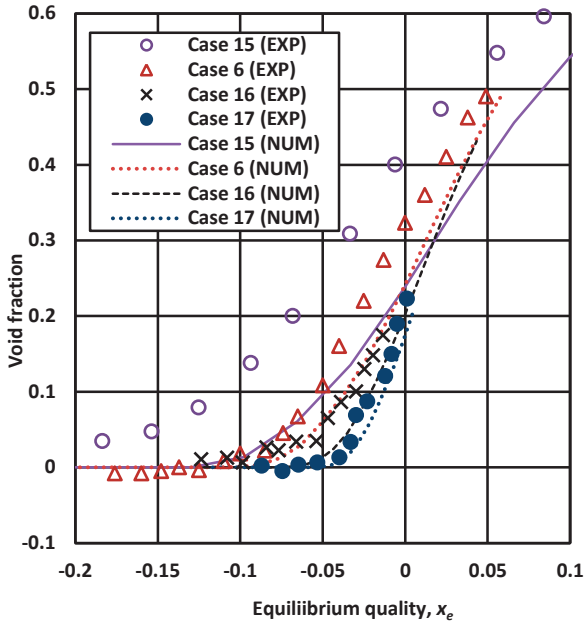

Fig. 5. Comparisons between numerical results (NUM) and experimental measurements (EXP), Group 4.

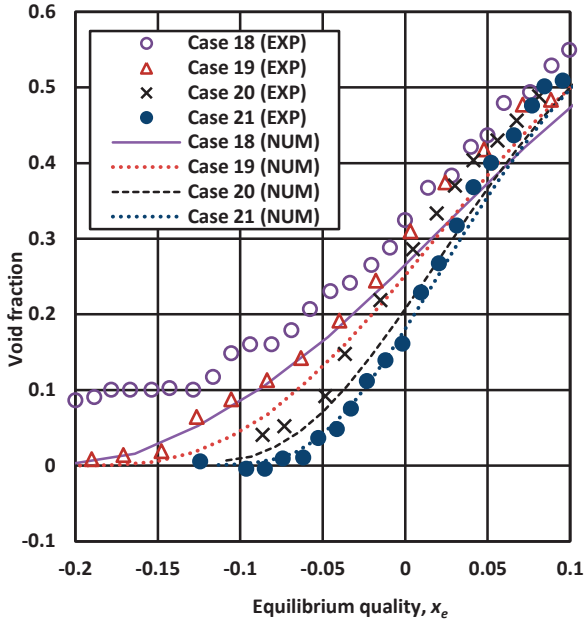

Fig. 6. Comparisons between numerical results (NUM) and experimental measurements (EXP), Group 5.

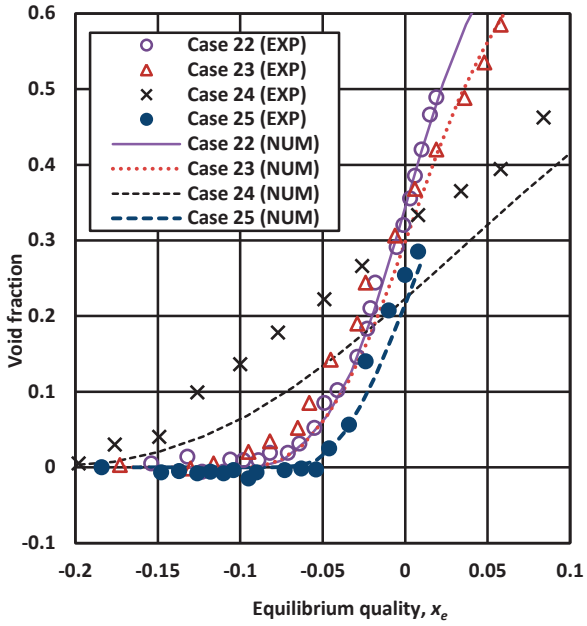

Fig. 7. Comparisons between numerical results (NUM) and experimental measurements (EXP), Group 6.

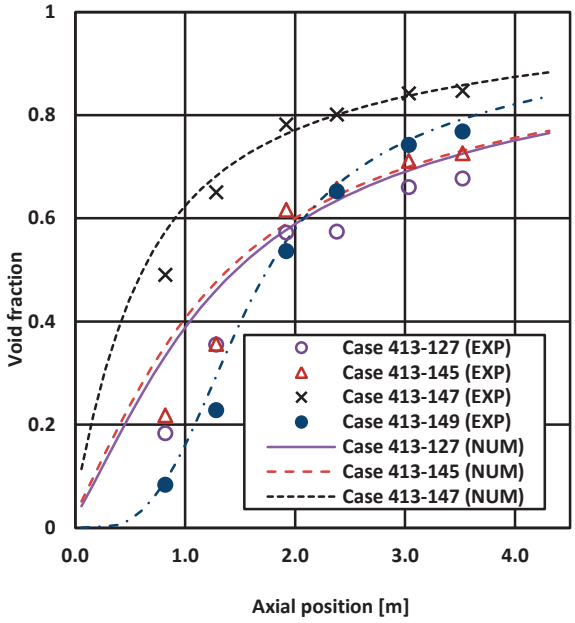

Fig. 8. Comparisons between numerical results (NUM) and experimental measurements (EXP), Group 7.

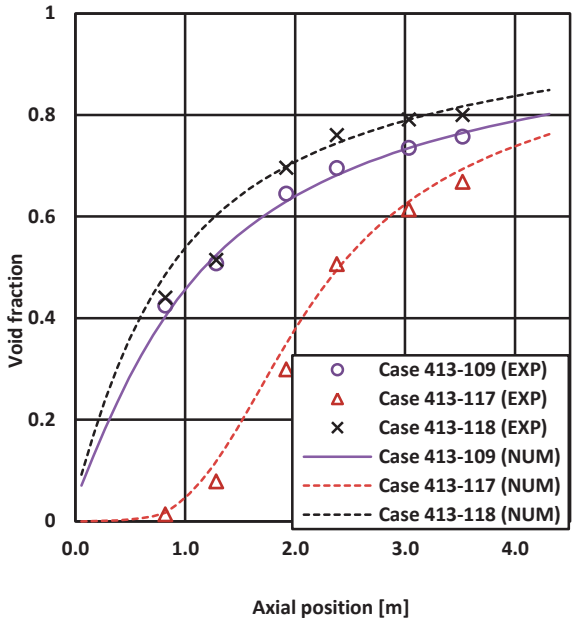

Fig. 9. Comparisons between numerical results (NUM) and experimental measurements (EXP), Group 8.

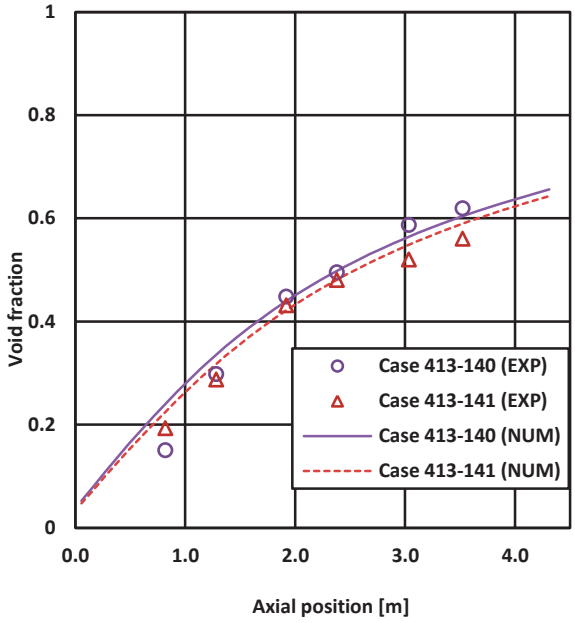

Fig. 10. Comparisons between numerical results (NUM) and experimental measurements (EXP), Group 9.

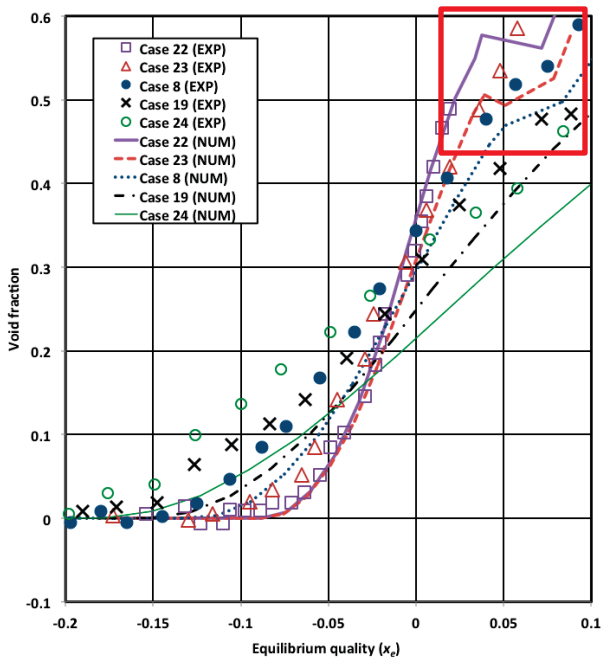

Fig. 11. Results obtained in previous work (Ref. 18). Comparisons between numerical results (NUM) and experimental measurements (EXP), for Bartolomei cases 8, 19, 22, 23, and 24.

V. CONCLUSIONS

We have successfully demonstrated the capability of applying the JFNK method to solve the two-phase four-equation drift flux model with the full coverage of all the flow regimes for vertical upward channels. The staggered grid finite volume method and fully implicit backward Euler method was used for the spatial discretization and time integration schemes, respectively. This work represents an extension to our previous work to resolve those unphysical behaviors observed in numerical results. The EPRI drift flux correlations used in this work provide continuous functions in the whole two-phase flow region, and thus those unphysical behaviors observed in our previous work are eliminated. Code validation was performed comparing the numerical results to subcooled flow boiling experimental data in both vertical pipe and rod bundle geometries. For most simulation cases, the numerical results agree well with experimental data.

ACKNOWLEDGMENTS

This work is supported by the United States (U.S.) Department of Energy, under Department of Energy Idaho Operations Office Contract DE-AC07-05ID14517. Accordingly, the U.S. Government retains a nonexclusive, royalty-free license to publish or reproduce the published form of this contribution, or allow others to do so, for U.S. Government purposes.

REFERENCES

1. N. ZUBER and J. A. FINDLAY, "Average Volumetric Concentration in Two-Phase Flow Systems," *Journal of Heat Transfer*, **87** (4), pp. 453-468 (1965).
2. M. ISHII, "One-dimensional drift-flux model and constitutive equations for relative motion between phases in various two-phase flow regimes," ANL-77-47, USA, (1977).
3. M. ISHII and T. HIBIKI, *Thermo-Fluid Dynamics of Two-Phase Flow*, Second Edition, Springer, (2011).
4. "RETRAN-3D – A Program for Transient Thermal-Hydraulic Analysis of Complex Fluid Flow Systems: Volume 1: Theory and Numerics (Revision 3)," NP-7450-V1R3, Electric Power Research Institute, October, (1998).
5. Y.J. CHUNG et al., "Development and Assessment of System Analysis Code, TASS/SMR for Integral Reactor, SMART," *Nuclear Engineering and Design*, **244**, pp. 52-60, (2012).
6. Y.J. CHUNG et al., "Applicability of TASS/SMR using drift flux model for SMART LOCA analysis," *Nuclear Engineering and Design*, **262**, pp. 228-234, (2013).
7. H.J. KHAN and H.C. YI, "Subchannel Analysis in BWR Fuel Bundles," *Annals of Nuclear Energy*, **Vol. 12**, No. 10, pp. 559-572, (1985).
8. M. HASHEMI-TILEHNOEE and M. RAHGOSHAY, "Benchmarking a Sub-channel Program based on a Drift-flux Model with 8×8 NUPEC BWR Rod Bundle," *Annals of Nuclear Energy*, **Vol. 58**, pp. 202-212, (2013).
9. M. HASHEMI-TILEHNOEE and M. RAHGOSHAY, "Sub-channel Analysis of 8×8 and 9×9 BWR Fuel Assemblies with Different Two-phase Flow Model," *Annals of Nuclear Energy*, **Vol. 62**, pp. 264-268, (2013).
10. J.D. GALLOWAY, "Boiling Water Reactor Core Simulation with Generalized Isotopic Inventory Tracking for Actinide Management", PhD Dissertation, University of Tennessee, Knoxville, (2010).
11. A.K. NAYAK, "Study on the Stability Behaviour of Two-phase Natural Circulation Systems using a Four-equation Drift Flux

Model," *Nuclear Engineering and Design*, **237**, pp. 386-398, (2007).
12. J. WANG et al., "Numerical Study of Nuclear Coupled Two-phase Flow Instability in Natural Circulation System under Low Pressure and Low Quality," *Nuclear Engineering and Design*, **241**, pp. 4972-4977, (2011).
13. V.A. MOUSSEAU, "Implicitly Balanced Solution of the Two-phase Flow Equations Coupled to Nonlinear Heat Conduction," *J. Comp. Phys.*, **200**, 104-132 (2004).
14. V.A. MOUSSEAU, "A Fully Implicit Hybrid Solution Method for a Two-Phase Thermal-Hydraulic Model", *Journal of Heat Transfer*, **Vol. 127**, 531-539 (2005).
15. RELAP-7 Theory Manual, INL/EXT-14-31366, February 2014, Idaho National Laboratory
16. RELAP-7 Level 2 Milestone Report: Demonstration of a Steady State Single Phase PWR Simulation with RELAP-7, INL/EXT-12-25924, May 2012, Idaho National Laboratory
17. D.R. GASTON, et al., "Physics-based multiscale coupling for full core nuclear reactor simulation", *Annuals of Nuclear Energy*, **Vol. 84**, 45-54, (2015).
18. L. ZOU, H. ZHAO and H. ZHANG, "Numerical Implementation, Verification and Validation of Two-phase Flow Four-equation Drift Flux Model with Jacobian-free Newton-Krylov Method," *Annals of Nuclear Energy*, **Vol. 87**, pp. 707-719, (2016).
19. L. ZOU, H. ZHAO and H. ZHANG, "Applications of High-resolution Spatial Discretization Scheme and Jacobian-free Newton-Krylov Method in Two-phase Flow Problems," *Annals of Nuclear Energy*, **Vol. 83**, pp. 101-107, (2015).
20. L. ZOU, H. ZHAO and H. ZHANG, "On the Analytical Solutions and Numerical Verifications of the Two-Phase Water Faucet Problem", 16th International Topical Meeting on Nuclear Reactor Thermalhydraulics (NURETH-16), Augst 30 – September 4, Chicago, Illinois, USA, 2015
21. L. ZOU, H. ZHAO and H. ZHANG, "Implicitly Solving Phase Appearance and Disappearance Problems Using Two-Fluid Six-Equation Model," *Progress in Nuclear Energy*, Paper Under Review, (2015).
22. B. CHEXAL and G. LELLOUCHE, A Full-Range Drift-Flux Correlation for Vertical Flows (Revision 1), EPRI NP-3989-SR, Electric Power Research Institute, September 1986.
23. T. HIBIKI and M. ISHII, "One-dimensional drift-flux model and constitutive equations for relative motion between phases in various two-phase flow regimes," *International Journal of Heat and Mass Transfer*, **Vol. 46**, 4935-4948, (2003).
24. "RELAP5-3D Code Manual Volume I: Code Structure, System Models and Solution Methods," INEEL-EXT-98-00834, Revision 4.0, June (2012).
25. "RELAP5-3D Code Manual Volume IV: Models and Correlations," INEEL-EXT-98-00834, Revision 4.0, June (2012).
26. S. BALAY et al., "PETSc Users Manual, Reversion 3.4," ANL-95/11 (2013).
27. G.G. BARTOLOMEI et al., "An Experimental Investigation of True Volumetric Vapor Content with Sub-cooled Boiling in Tubes," *Thermal Engineering* **29 (3)**, 132–135, (1982).
28. J.A. SKAUG, R. EKLUND, and O. NYLUND, "FT-36b: Results of Void Measurements," FRIGG Loop Project, FRIGG-PM--15, (1968).